Available online at www.sciencedirect.com
ScienceDirect
Journal of Molecular Catalysis A: Chemical 261 (2007) 225–231
JOURNAL OF MOLECULAR CATALYSIS A: CHEMICAL
www.elsevier.com/locate/molcata

Short communication

Synthesis, characterization and catalytic application of Cr–SBA-1 mesoporous molecular sieves

Xinhong Zhao [a,b], Xiaolai Wang [a,*]

[a] *State Key Laboratory for Oxo Synthesis and Selective Oxidation, Lanzhou Institute of Chemical Physics, Chinese Academy of Sciences, Lanzhou 730000, PR China*
[b] *The Graduate University of the Chinese Academy of Sciences, Beijing 10039, PR China*

Received 20 September 2005; accepted 2 August 2006
Available online 11 September 2006

Abstract

A series of Cr–SBA-1 (*Pm*3*n*) mesoporous molecular sieves were directly synthesized under strongly acidic conditions using ammonium dichromate as chromium source and characterized by various techniques. X-ray diffraction (XRD) showed that the synthesized mesoporous materials had a well-ordered cubic structure. N_2 adsorption/desorption measurements confirmed that the resultant samples had large mesopores (>23 Å) and highly surface areas (>1000 $m^2\,g^{-1}$). FT-IR and UV–vis results revealed that both monochromate and polychromate coexisted on these mesoporous materials. All these samples prepared by direct synthesis have been used as catalysts for dehydrogenation of ethane with carbon dioxide. Among these catalysts, Cr–SBA-1(III) exhibited the highest catalytic performance, giving 21.2% of ethylene yield with a selectivity of 86.9% at 650 °C, whereas, its catalytic activity is lower than that of Cr–SBA-1 prepared by conventional impregnation.

Keywords: Cr–SBA-1; Mesoporous materials; Ethane; Carbon dioxide; Dehydrogenation; Cr–SBA-1

1. Introduction

The discovery of ordered materials with pore sizes in the mesopore range by researchers of the Mobil Oil Company [1,2] has initiated an intensive research effort resulting in more than 3000 publications. Among these materials, only little information is available on the synthesis of the cubic phase MCM-48 (*Ia3d* cubic). The lack may be due to the difficulty of its preparation compared to that of MCM-41 [3,4]. In the last decade, Huo et al. reported the synthesis of SBA-1 under strongly acidic conditions employing a so-called $S^+X^-I^+$ mechanism [5–7]. SBA-1 is a cubic phase, which possesses a three-dimensional cage-type structure. Pure silica mesoporous materials possess a neutral framework, which limits their application in catalysis. To obtain materials with potential for catalytic applications, it is necessary to modify the nature of the amorphous walls by incorporation of hetero elements. Recently, the incorporation of Ti, V, Fe, Co and Mo into SBA-1 mesoporous materials has been reported [8–13]. The development of ordered mesoporous materials containing different atoms in the framework has opened up new possibilities for the use of mesoporous molecular sieve materials in the field of catalysis.

Chromium-containing mesoporous molecular sieves have received much attention because of their wide use in many catalytic reactions. In recent years, a series of chromium-containing mesoporous molecular sieves, including Cr-MCM-41 [14–16] and Cr-HMS [17] have been synthesized and used as catalysts for various catalytic reactions. However, up to now, only a few studies have been reported on SBA-1, as compared with the number of studies on those chromium-containing mesoporous materials. Because of the cubic structure of three-dimensional mesopores of SBA-1, it has greater potential in catalytic applications than the one-dimensional mesoporous material.

In the present paper, we report the preparation of Cr–SBA-1 molecular sieves by the direct synthesis. A systematic investigation of the above materials are carried out for their characterizations by powder X-ray diffraction (XRD), nitrogen adsorption/desorption, Fourier transform infrared spectroscopy

* Corresponding author. Tel.: +86 931 8275727; fax: +86 931 8277787.
E-mail addresses: fpierc@lzb.ac.cn (X. Wang), Licpzhaoxh@yahoo.com.cn (X. Zhao).

1381-1169/$ – see front matter © 2006 Elsevier B.V. All rights reserved.
doi:10.1016/j.molcata.2006.08.008

(FT-IR) and diffuse reflectance UV–visible (UV–vis) spectroscopy. All these mesoporous materials will be used as catalysts for the dehydrogenation of ethane with carbon dioxide. Cr–SBA-1 prepared by conventional impregnation method, which was considered as a reference sample, was also used to the dehydrogenation of ethane by carbon dioxide.

2. Experimental

2.1. Synthesis of mesoporous materials

Cubic mesoporous molecular sieves Cr–SBA-1 were synthesized under acidic conditions using cetyltriethylammonium bromide ($C_{16}H_{33}(C_2H_5)_3NBr$, CTEABr) as a template, tetraethyl orthosilicate ($Si(OC_2H_5)_4$, TEOS, Aldrich, 98%) as a silica source and ammonium dichromate ($(NH_4)_2Cr_2O_7$, Acros, 99%) as a chromium source in aqueous solution of hydrochloric acid. The surfactant CTEABr was synthesized by the reaction of cetylbromide with an excessive amount of triethylamine in acetone solution under reflux conditions for 5 days. The resulting CTEABr was purified five times by recrystallization from acetone solution.

In a typical synthesis of the Cr–SBA-1, 2.64 g (6.5 mmol) of CTEABr, 162 ml (9.0 mol) of distilled water and 83.6 ml hydrochloric acid (1 mol, Aldrich, 37%) were combined with a desired amount of ammonium dichromate to form a homogeneous solution, which was cooled at 0 °C and stirred for 30 min. Then 10.4 g (50 mmol) of TEOS (precooled to 0 °C) was added to the above mixture with vigorous stirring. The molar composition of the reaction mixture was 1.0TEOS:0.13CTEABr:20HCl:250H_2O:(0.01–0.08)Cr. After being stirred for 3 min, the above mixture was allowed to react at 0 °C under static condition for 8 h. The resultant precipitates were filtered and dried (without washing) at 100 °C overnight, and then calcined in a flow of air at 600 °C for 4 h. Pure siliceous SBA-1 was synthesized with the same procedure except that no Cr was added. Supported chromium catalysts on SBA-1 (Cr–SBA-1) was prepared by impregnation method using ammonium dichromate as the Cr source, and then dried at 100 °C overnight and calcined at 600 °C for 4 h.

2.2. Catalyst characterizations

The amount of Cr was quantified by inductively coupled plasma emission spectrometry. The measurements were performed with a Rigaku JY38S, and the sample was dissolved in a mixture of HF and HNO_3 acids before the measurements. Powder X-ray diffraction (XRD) patterns of the synthesized mesoporous materials were recorded on a D/Max-2400 Rigaku diffractometer with Cu Kα radiation operated at 40 kV and 60 mA. The diffraction data were collected by using a continuous scan mode with a scan speed of 1.2° (2θ) min^{-1}. Nitrogen adsorption/desorption isotherms were measured at −196 °C on a Micromeritics ASAP2010 instrument. Samples were outgassed at 200 °C and 10^{-2} Pa over night before measurements. Surface areas were calculated using the BET method. The primary mesopore volume V_p was obtained using the high-resolution *t*-plot method. The pore size distributions were obtained from adsorption branches of isotherms using the BJH method. FT-IR spectroscopy was carried out on a Bruker IFS 120 FT-IR spectrometer using ca. 0.5 mm KBr pellets containing 2.5 mass% sample. Diffuse reflectance UV–vis spectroscopic measurements were recorded on a Shimadzu UV-240 recording spectrometer. The spectra were collected at 200–700 nm referenced to $BaSO_4$. Temperature programmed reduction (TPR) experiments were carried out in a fixed bed reactor loaded with 0.05 g samples. The samples were reduced in 10% H_2/Ar flow at a rate of 30 ml/min from ambient temperature to 700 °C at a heating rate of 10 °C/min. Before TPR the samples were pretreated under Ar gas flow of 30 ml/min to 300 °C at a heating rate of 5 °C/min and then further treated at the same temperature for 30 min. The concentrations of H_2 were determined by a GC-7890 gas chromatograph equipped with a TCD. To calibrate the amount of H_2 consumption, the CuO powder supplied by Merck was used.

2.3. Catalytic reactions

The oxidative dehydrogenation of ethane with carbon dioxide was carried out using a fixed bed flow-type quartz reactor (i.d. 8 mm × 180 mm) at atmosphere pressure. Four hundred milligrams of a catalyst, 12 ml/min C_2H_6 and 48 ml/min of CO_2 were introduced. The products were analyzed with on-line GC-7890 gas chromatograph (TianMei, ShangHai, China) equipped with a 3 mm × 3 m stainless steel column packed with Poropack Q using H_2 as a carrier gas. The conversion and selectivity were calculated as follows:

$$C_2H_6 \text{ conversion} = \frac{1 - 2n_{C_2H_6}}{2n_{C_2H_6} + 2n_{C_2H_4} + n_{CH_4}}$$

$$C_2H_4 \text{ selectivity} = \frac{2n_{C_2H_4}}{2n_{C_2H_4} + n_{CH_4}}$$

All the experimental data were corrected after the reaction for 0.5 h. Moreover, the reaction data in the work were reproducible with a precision of less than 5%.

3. Results and discussion

Fig. 1 illustrates the X-ray diffraction (XRD) patterns of the calcined siliceous SBA-1 and various Cr–SBA-1 samples prepared by direct synthesis. As Fig. 1 displays, the four samples (Fig. 1a–d) show an intense (2 1 0) reflection and smaller (2 0 0) and (2 1 1) reflections in the region of $2\theta = 1.5$–3°. The characteristic XRD pattern exhibited by the SBA-1 cubic phase (which can be indexed to *Pm3n* space group) matches well with those reported in the literature [5–7]. However, the decrease in intensity of (2 0 0) and (2 1 1) reflections with increasing n_{Cr}/n_{Si}, suggests that higher amount of chromium incorporation in the mesoporous materials might reduce the structural order. Table 1 summarizes the preparation conditions and physical properties of the resultant Cr–SBA-1 mesoporous molecular sieves, together with the data of Cr–SBA-1 for comparison. It is interesting to note there is no evident difference in the intensity of the (2 1 0) peak and the unit-cell parameter ($a_0 = d_{2\,1\,0}\sqrt{5}$)

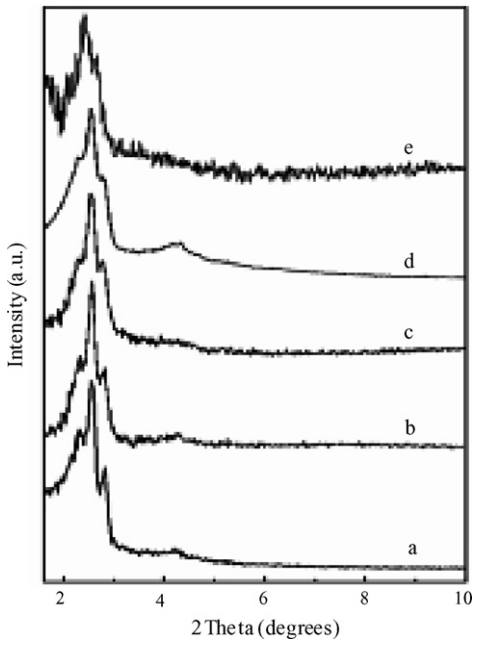

Fig. 1. XRD patterns of the various calcined samples: (a) siliceous SBA-1; (b) Cr–SBA-1(I); (c) Cr–SBA-1(II); (d) Cr–SBA-1(III); (e) Cr–SBA-1(IV).

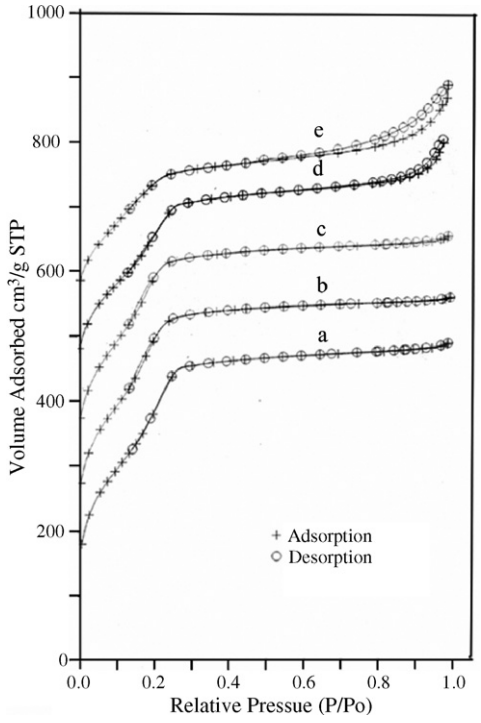

Fig. 2. N_2 adsorption/desorption isotherms of the various calcined samples: (a) siliceous SBA-1; (b) Cr–SBA-1(I); (c) Cr–SBA-1(II); (d) Cr–SBA-1(III); (e) Cr–SBA-1(IV).

between calcined Cr–SBA-1 and a siliceous SBA-1. This is consistent with what would be expected because the Cr–O bond length is almost identical to that of Si–O. With the molar ratio of HCl/TEOS = 20 in the synthesized precursor, the Cr–SBA-1 sample containing up to 3.75 wt.% Cr ($n_{Cr}/n_{Si} = 0.04$) is formed while still maintaining a fairly well-ordered cubic structure, this can be explained by the results of Dai, who reported that anionic Mo and V species favored the incorporation of Mo and V into the SBA-1 framework according to the $S^+X^-I^+$ synthesis route [9,12].

The N_2 adsorption/desorption isotherms and their corresponding pore size distribution curves for the calcined siliceous SBA-1 and various Cr–SBA-1 samples are shown in Figs. 2 and 3. As Fig. 2 displays, the isotherms for these samples are type IV adsorption isotherms typical of mesoporous solids. Adsorption at low pressures ($P/P_0 < 0.15$) is accounted for by monolayer–multilayer adsorption of N_2 on the walls of the mesopores. At a relative pressure P/P_0 between 0.15 and 0.30, the isotherms exhibit a sharp inflection characteristic of capillary condensation within the mesopores. The sharpness in this step indicates a uniform pore size. For Cr–SBA-1(III) and Cr–SBA-1(IV) an obvious hysteresis loop at $P/P_0 = 0.8$–1.0, which indicates that larger pores are filled at higher relative

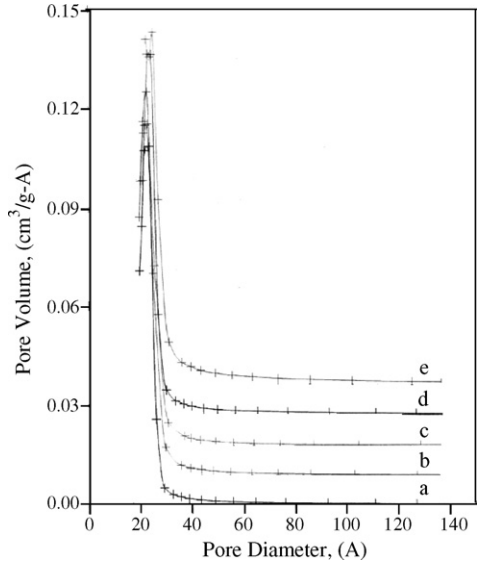

Fig. 3. Pore size distribution of the various calcined samples: (a) siliceous SBA-1; (b) Cr–SBA-1(I); (c) Cr–SBA-1(II); (d) Cr–SBA-1(III); (e) Cr–SBA-1(IV).

Table 1
Synthesis conditions and physico-chemical properties of various calcined samples

Sample	Cr/Si in gel	Cr amount (wt.%)	a_0 (Å)	S_{BET} ($m^2\ g^{-1}$)	Pore diameter (Å)	Pore volume ($cm^3\ g^{-1}$)
SBA-1	–	0.00	74.9	1417	24.1	0.71
Cr–SBA-1(I)	0.01	0.88	75.6	1363	23 2	0.55
Cr–SBA-1(II)	0.02	1.81	76.2	1297	23.7	0.50
Cr–SBA-1(III)	0.04	3.75	75.9	1228	28.4	0.43
Cr–SBA-1(IV)	0.08	7.39	76.1	871	32.6	0.36
Cr/SBA-1	–	3.71	–	1000	24.5	0.22

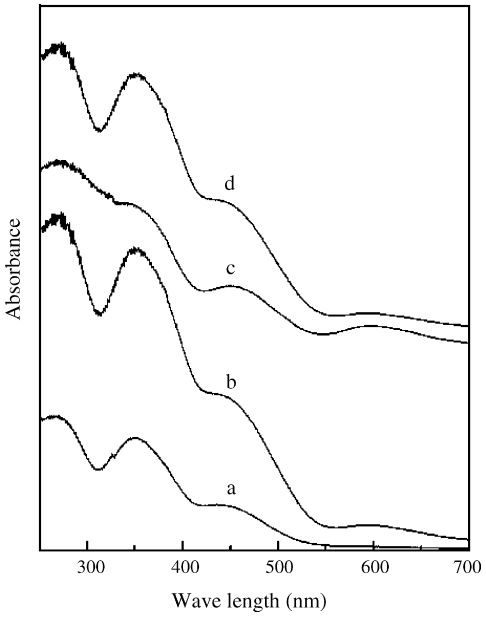

Fig. 4. UV–vis diffuse reflectance spectra of various calcined Cr–SBA-1 samples: (a) Cr–SBA-1(I); (b) Cr–SBA-1(II); (c) Cr–SBA-1(III); (d) Cr–SBA-1(IV).

pressures, is also observed. Both siliceous SBA-1 and various Cr–SBA-1 samples showed a uniform pore size distribution with a pore diameter of 23–33 Å as calculated by the BJH method. The BET surface area, BJH pore size and pore volume of the samples are listed in Table 1. A slight decrease in the mesoporous surface areas and pore volumes with increasing chromium content is caused by the incorporation of chromium. This can be explained by some destruction of the pore structure of Cr–SBA-1 materials, which is in agreement with the results of XRD shown in Fig. 1.

Fig. 4 shows the UV–vis diffuse reflectance spectra of the calcined Cr–SBA-1 with different n_{Cr}/n_{Si} synthesized by direct synthesis. UV bands at 265 and 350 nm, which could be assigned to O–Cr(VI) charge transfers of chromate species [18], are observed for all the samples. A shoulder around 450 nm assigned to Cr(VI) polychromate is also observed for the four Cr–SBA-1 samples. However, a band at 600 nm assigned to octahedral Cr(III) in Cr_2O_3 or CrO_x clusters is not observed for Cr–SBA-1(I) with lower chromium content, while for the other three samples with higher chromium content the band is detected. These results indicate that both Cr(VI) monochromate and polychromate coexist in calcined Cr–SBA-1, and octahedral Cr(III) in Cr_2O_3 or CrO_x clusters also exists when chromium content is above 1.81 wt.%.

Fig. 5 shows FT-IR spectra of calcined siliceous SBA-1 and various Cr–SBA-1 samples. The band at 905 cm^{-1} in the group of Cr–SBA-1 samples can be assigned to Cr–O or Cr=O vibration from Cr(VI) species as reported earlier [19]. Moreover, the optical density of this band, which is absent in calcined siliceous SBA-1, increases with the increase of Cr content. The peaks near 1089 and 802 cm^{-1} correspond to asymmetric and symmetric vibrations of Si–O–Si linkage, respectively. In all samples a FT-IR band around 960 cm^{-1} is observed, which is often assigned to a lattice defect and is correlated with the presence of chromium

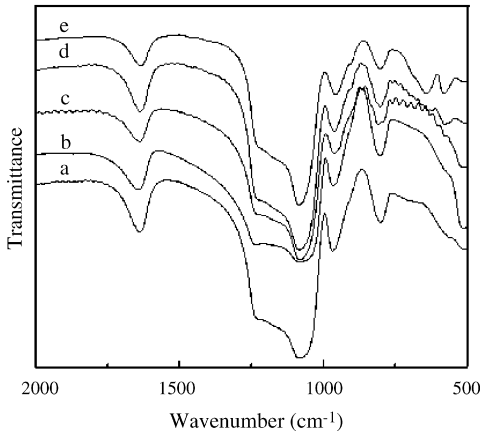

Fig. 5. FT-IR spectra of the various calcined samples: (a) siliceous SBA-1; (b) Cr–SBA-1(I); (c) Cr–SBA-1(II); (d) Cr–SBA-1(III); (e) Cr–SBA-1(IV).

ions (or other framework ions) in a chromium silicate-1 framework (CrS-1) [20]. This 960 cm^{-1} band is also prominent in the FT-IR spectrum of calcined siliceous SBA-1. By carefully examining this band, it is at 966 cm^{-1} in siliceous SBA-1 and is shifted to 956 cm^{-1} in Cr–SBA-1(IV) shown in Fig. 5. Recent work suggests that this band is assignable to a Si–O vibration in a Si–OH group in siliceous MCM-41 [21]. If this is the case, it is reasonable to attribute the red shift in Cr–SBA-1 to the replacement of a OH group by O–Cr(VI). The bands at 623 and 569 cm^{-1} are found to be due to extra framework chromium oxide as reported earlier [22]. These bands are found to be absent in siliceous SBA-1 where Cr is not incorporated.

Fig. 6 shows the TPR profiles of various calcined Cr–SBA-1 and Cr–SBA-1 samples. No clear reduction peaks are observed for pure siliceous SBA-1 while one or two reduction peaks

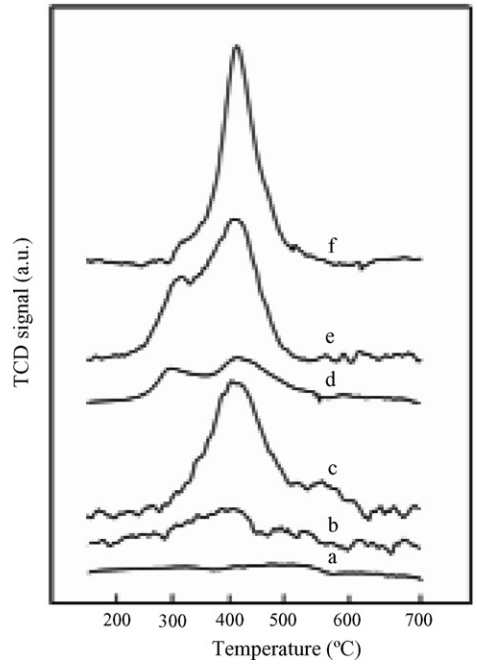

Fig. 6. TPR profiles of various calcined Cr–SBA-1 and Cr/SBA-1 samples: (a) siliceous SBA-1; (b) Cr–SBA-1(I); (c) Cr–SBA-1(II); (d) Cr–SBA-1(III); (e) Cr–SBA-1(IV); (f) Cr/SBA-1.

Table 2
Results of homogeneous reaction between ethane and CO_2 at various temperatures

Temperature (°C)	Conversion (%)		C_2H_4 yield (%)	Selectivity (%)	
	C_2H_6	CO_2		C_2H_4	CH_4
600	0	0	0	0	0
650	1.91	0	1.87	97.7	2.3
700	5.19	0	4.95	95.4	4.6
750	21.8	0	21.4	93.5	6.5
800	55.9	0	50.9	91.0	9.0

Reaction conditions: SV = 9000 h^{-1} ml/g-cat. $V(C_2H_6)/V(CO_2)$ = 12/48.

appear in the group of Cr–SBA-1 samples. Therefore the reduction peaks of these Cr–SBA-1 samples must be related with the presence of reducible chromium species. For Cr–SBA-1(III) and Cr–SBA-1(IV), the consumption of hydrogen observed at low temperature (290 °C) could be attributed to the reduction of polychromate to $Cr^{III}O_x$. The second band at higher temperature (400 °C) is assigned to the reduction of monochromate to $Cr^{III}O_x$ [14,18]. It is noteworthy that only one reduction peak at higher temperature is observed for Cr–SBA-1(I) and Cr–SBA-1(II), although both monochromate and polychromate coexist on the surface of the two samples. We speculate that the reduction peak at higher temperature may overlap that at lower temperature in the case of Cr–SBA-1(I) and Cr–SBA-1(II) based on the results of Weckhuysen et al. [18], who reported that monochromate was the dominated species at lower chromium content for Cr-supported catalysts.

3.1. Catalytic tests

Table 2 lists the results of homogeneous reaction between ethane and CO_2. It was seen that this reaction could not be carried out at 600 °C. When the reaction temperature was above 650 °C ethane conversion and ethylene yield significantly increased with the increasing temperature. On the other hand, CO_2 conversion was zero and CO was not detected in the whole range of temperatures studied. Therefore, the homogeneous reaction of ethane and CO_2 was mainly an ethane dehydrogenation, as ethylene was a primary product (selectivity above 91.0%) and a minor amount of methane is a secondary product produced by thermal cracking of ethane at the higher temperatures. These results were consistent with those of literatures [23,24]. In the present paper, we restricted the reaction temperature below 650 °C. Under this reaction condition, the homogeneous reaction between ethane and CO_2 is negligible.

Fig. 7 shows the effect of chromium content in the Cr–SBA-1 system on catalytic performance at 650 °C. When Cr–SBA-1 mesoporous molecular sieves with different n_{Cr}/n_{Si} ratios were used as the catalysts for the dehydrogenation of ethane with carbon dioxide, the conversion of ethane increased almost linearly with increasing Cr content from 0% to 3.75% and it reached the maximum value at 3.75 wt.%Cr, whereas, ethane conversion decreased slightly when Cr content was increased up to 7.39%. The selectivity towards ethylene over Cr–SBA-1 catalysts is lower than that of pure siliceous SBA-1, however, it shows little difference among Cr–SBA-1 catalysts with the varying Cr

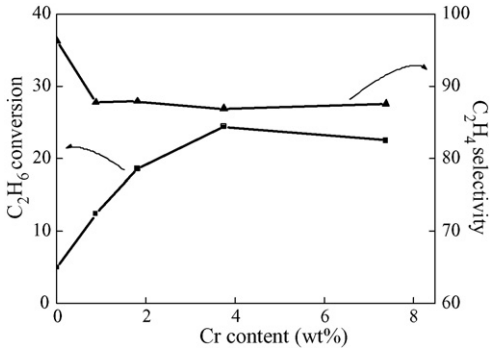

Fig. 7. Effects of Cr content in Cr–SBA-1 system on catalytic performance. Reaction conditions: 650 °C, SV = 9000 h^{-1} ml/g-cat. $V(C_2H_6)/V(CO_2)$ = 12/48.

content. Among these catalysts, Cr–SBA-1(III) exhibited the highest catalytic performance, giving 21.2% of ethylene yield with a selectivity of 86.9% at 650 °C.

Fig. 8 shows the catalytic properties of Cr–SBA-1(III) and Cr/SBA-1 catalysts for the dehydrogenation of ethane with carbon dioxide at various temperatures. It was seen that the conversion of ethane increased almost linearly with the increasing temperature for the two samples, whereas, selectivity to ethylene decreased slightly. On the other hand, we can see that Cr/SBA-1 catalyst showed higher ethane conversion and similar selectivity towards ethylene in comparison to that of Cr–SBA-1(III) in the whole range of temperatures studied.

It has been proposed that the active species for dehydrogenation of light alkanes in chromium-based catalysts are Cr^{3+} ion. Wang et al. studied the dehydrogenation of propane with carbon dioxide on Cr-MCM-41 prepared by direct hydrothermal synthesis and template-ion exchange. They suggested that aggregated Cr(III) species was responsible for the dehydrogenation of propane [14]. Nakagawa et al. investigated the dehydrogenation of ethane in the presence of carbon dioxide over Cr/diamond catalyst and proposed that Cr_2O_3 or a higher-oxidation state of chromium oxides were active species [25]. Wang et al. evaluated the same reaction over Cr/SiO_2 catalyst. They found that two Cr species, Cr^{3+} and Cr^{6+}, coexisted on the catalyst surface. Thus, they believed that surface Cr^{3+} species and Cr^{6+}/Cr^{3+} were the active sites for dehydrogenation of ethane based on XPS and TPR measurements [26,27]. In our case, we found

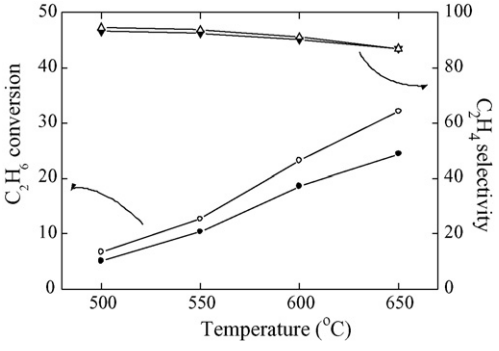

Fig. 8. Dehydrogenation of C_2H_6 with CO_2 over Cr/SBA-1 (empty symbols) and Cr/SBA-1(III) (full symbols) at various temperatures. Reaction conditions: SV = 9000 h^{-1} ml/g-cat. $V(C_2H_6)/V(CO_2)$ = 12/48.

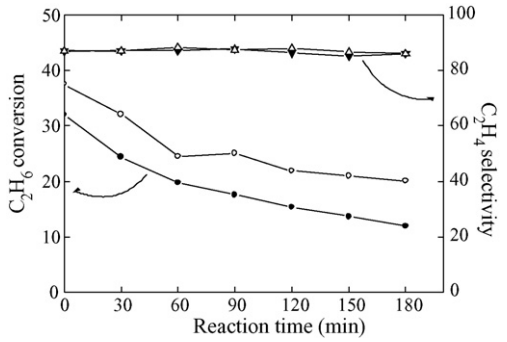

Fig. 9. Stability of Cr/SBA-1 (empty symbols) and Cr/SBA-1(III) (full symbols). Reaction conditions: 650 °C; SV = 9000 h^{-1} ml/g-cat. $V(C_2H_6)/V(CO_2)$ = 12/48.

that only monochromate species existed on the impregnated Cr/SBA-1 while several types of chromate species including both monochromate and polychromate coexisted on Cr–SBA-1(III). This result demonstrated that chromium was more highly dispersed in Cr/SBA-1 than that in Cr–SBA-1(III). The X-ray diffraction patterns of Cr/SBA-1 and Cr–SBA-1(III) (not shown) at $2\theta = 10–70^\circ$ also indicated that Cr/SBA-1 exhibited higher dispersion degree of chromium species in comparison to Cr–SBA-1(III). Above observation can be explained by the state of chromium oxoanion in the direct synthesis and impregnation solutions. As mentioned in Section 2, the Cr–SBA-1(III) was synthesized under highly acidic conditions (pH < 0), and Cr/SBA-1 was prepared by impregnation with an aqueous solution of ammonium dichromate at pH 6. In aqueous solutions of chromium anions, different equilibrium phases exist, depending on the pH [18].

$$2CrO_4^{2-} + 2H^+ \leftrightarrow Cr_2O_7^{2-} + H_2O \quad (2 < pH < 6) \qquad (1)$$

$$2Cr_2O_7^{2-} + 2H^+ \leftrightarrow Cr_4O_{13}^{2-} + H_2O \quad (pH < 2) \qquad (2)$$

At pH < 0, i.e., the Cr–SBA-1(III) synthesis conditions, the chromium anions are present as large polyanions; the pH was low enough to convert the most of $[Cr_2O_7]^{2-}$ into $[Cr_4O_{13}]^{2-}$ through Eq. (2), resulting in poor dispersion on the silica surface. In the pH range of 2–6, i.e., the Cr/SBA-1 impregnation conditions, the chromium anions is smaller than under low pH conditions, which leads to a better dispersion of Cr oxide on SBA-1 surface.

The redox properties of Cr/SBA-1 and Cr–SBA-1(III) are shown in Fig. 6. It was noticeable that the profile of Cr/SBA-1 catalyst showed a pronounced H_2 consumption peak attributed to the reduction of monochromate to $Cr^{III}O_x$. However, two small peaks were detected for the Cr–SBA-1(III) catalyst, which could be attributed to the reductions of polychromate to $Cr^{III}O_x$ and monochromate to $Cr^{III}O_x$, respectively. It was thus reasonable to speculate that such Cr(III) species were responsible for the dehydrogenation of ethane by carbon dioxide. Based on the above results, the different catalytic behavior between Cr/SBA-1 and Cr–SBA-1(III) can be explained.

Fig. 9 shows the catalytic performance of Cr/SBA-1 and Cr–SBA-1(III) catalysts as a function of time. It was seen that the two catalysts exhibited obvious deactivation with increasing the reaction time. However, deactivation rates were different over the two catalysts. Cr–SBA-1(III) showed a higher deactivation rate. Ethane conversion decreased from 37.5% to 20.1% for Cr/SBA-1 catalyst after about 3 h reaction. For Cr–SBA-1(III), ethane conversion changed from 32.0% to 12.0% after about 3 h. For both catalysts, as ethane conversion decreased, ethylene selectivity was kept at 85–87%.

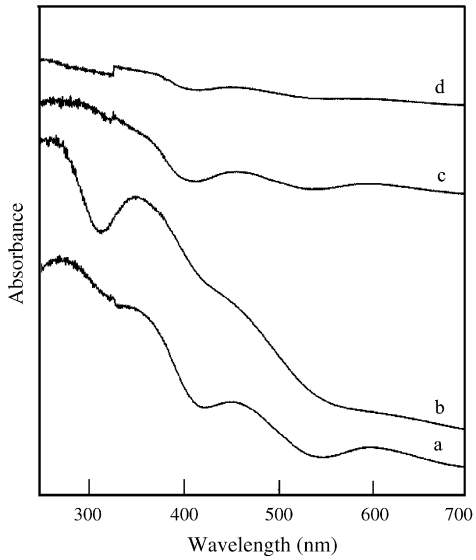

Fig. 10. UV–vis diffuse reflectance of Cr–SBA-1(HI) and Cr/SBA-1: (a) fresh Cr–SBA-1(III); (b) fresh Cr/SBA-1; (c) Cr–SBA-1(III) after the reaction for 3 h under CO_2; (d) Cr/SBA-1 after the reaction for 3 h under CO_2.

Takehira and Ohishi investigated the deactivation mechanism of Cr-MCM-41 catalysts during the dehydrogenation of propane and ethylbenzene with CO_2, suggesting that Cr(VI) in tetrahedral coordination formed as an active monochromate species and reduced to Cr(III) in octahedral coordination as a less active polychromate species during the two reactions [28,29]. Takahara et al. studied the deactivation behavior of Cr_2O_3/SiO_2 during the dehydrogenation of propane in the presence of CO_2; they proposed that the slower deactivation of the catalyst could attribute to the reason that CO_2 might maintain the surface of Cr_2O_3/SiO_2 to be partially oxidized during the reaction [30]. In this investigation, we found that UV bands at 265 and 350 nm assigned to O–Cr(VI) charge transfers of monochromate species could not be distinguished clearly for Cr/SBA-1 and Cr–SBA-1(III) catalysts after the dehydrogenation of ethane with CO_2 for 3 h (Fig. 10). Moreover, the optical intensities of the bands significantly decreased in comparison to that of fresh catalysts. Thus, it was concluded that tetrahedrally coordinated Cr(VI)O_4 existing on fresh Cr/SBA-1 and Cr–SBA-1(III) catalysts was reduced to octahedrally coordinated Cr(III) during the reaction. We believed that such change in the valence state of chromium caused the deactivation of Cr/SBA-1 and Cr–SBA-1(III) catalysts.

4. Conclusions

Cr-incorporated SBA-1 cubic mesoporous molecular sieves were successfully synthesized under strongly acidic conditions. Both monochromate and polychromate coexisted on these meso-

porous materials. Among these samples, Cr–SBA-1(III) exhibited the highest catalytic performance for the dehydrogenation of ethane with CO_2, whereas, its catalytic activity is lower than that of Cr/SBA-1 prepared by conventional impregnation. The difference of catalytic performance between Cr–SBA-1(III) and Cr/SBA-1 was related with the dispersion degrees and redox properties of chromium species. The two catalysts exhibited obvious deactivation with the increase of reaction time during this reaction, which could attribute to the reduction of tetrahedrally coordinated $Cr(VI)O_4$.

References

[1] C.T. Kresge, M.E. Leonowicz, W.J. Roth, J.C. Vartuli, J.S. Beck, Nature 359 (1992) 710.
[2] J.S. Beck, J.C. Vartuli, W.J. Roth, M.E. Leonowicz, C.T. Kresge, K.T. Schmitt, C.T. Chen, D.H. Olson, E.W. Sheppard, S.B. McCullen, J.B. Higgins, J.L. Schlenker, J. Am. Chem. Soc. 114 (1992) 10834.
[3] R. Schmidt, M. Stocker, D. Akporiaye, E.H. Torstad, A. Olsen, Micropor. Mater. 5 (1995) 1.
[4] K.A. Koyano, T. Tatsumi, J. Chem. Soc., Chem. Commun. (1996) 145.
[5] Q. Huo, D.I. Margolese, U. Ciesla, D.G. Demuth, P. Feng, T.E. Gier, P. Sieger, A. Firouzi, B.F. Chmelka, F. Schüth, G.D. Stucky, Chem. Mater. 6 (1994) 1176.
[6] Q. Huo, R. Leon, P.M. Petroff, G.D. Stucky, Science 268 (1995) 1324.
[7] Q. Huo, D.I. Margolese, G.D. Stucky, Chem. Mater. 8 (1996) 1147.
[8] D.J.R. Zhao, G. Lv, G. Qian, L. Yan, J. Suo, Appl. Catal. A 281 (2005) 39.
[9] L. Dai, K. Tabata, E. Suzuki, T. Tatsumi, Chem. Mater. 13 (2001) 208.
[10] A. Vinu, T. Krithiga, V. Murugesan, M. Hartmann, Adv. Mater. 16 (2004) 1817.
[11] A. Vinu, J. Dědeček, V. Murugesan, M. Hartmann, Chem. Mater. 14 (2002) 2433.
[12] L. Dai, K. Tabata, E. Suzuki, T. Tatsumi, Micropor. Mesopor. Mater. 44/45 (2001) 573.
[13] S. Che, Y. Sakamoto, H. Yoshotake, O. Terasaki, T. Tatsumi, J. Phys. Chem. B 105 (2001) 10565.
[14] Y. Wang, Y. Ohishi, T. Shishido, Q. Zhang, W. Yang, Q. Guo, H. Wan, K. Takehira, J. Catal. 220 (2003) 347.
[15] K. Takehira, Y. Ohishi, T. Shishido, T. Kawabata, K. Takaki, Q. Zhang, Y. Wang, J. Catal. 224 (2004) 404.
[16] Y. Ohishi, T. Kawabata, T. Shishido, K. Takaki, Q. Zhang, Y. Wang, K. Takehira, J. Mol. Catal. A 230 (2005) 49–58.
[17] H. Yamashita, K. Yoshizawa, M. Ariyuki, S. Higashimoto, M. Che, M. Anpo, J. Chem. Soc., Chem. Commun. (2001) 435.
[18] B.M. Weckhuysen, I.E. Wachs, R.A. Schoonheydt, Chem. Rev. 96 (1996) 3327.
[19] M.A. Vuurman, I.E. Wachs, D.J. Stufkens, A.J. Oskam, J. Mol. Catal. 80 (1993) 209.
[20] T. Chapus, A. Tuel, Y. Taarit, C. Naccache, Zeolites 14 (1994) 360.
[21] S. Schwarz, D.R. Corbin, A.J. Vega, in: R.F. Lobo, J.S. Beck, S.L. Suib, D.R. Corbin, M.E. Davis, L.E. Iton, S.I. Zones (Eds.), Proceedings of the Materials Research Society Symposium, vol. 431, Materials Research Society, Pittsburgh, PA, 1996, p. 137.
[22] J.A. Gadsden, Infrared Spectra of Minerals and Related Inorganic Compounds, Butterworth and Co. Publishers Ltd., 1975, p. 44.
[23] R.X. Valenzuela, G. Bueno, V.C. Corberán, Y. Xu, C. Chen, Catal. Today 61 (2000) 43.
[24] Y.D. Xu, C.C. Vicente, Prog. Nat. Sci. 10 (2000) 22.
[25] K. Nakagawa, C. Kajita, N. Ikenaga, T. Suzuki, T. Kobayashi, M. Nishitani-Gamo, T. Ando, J. Phys. Chem. B 107 (2003) 4048.
[26] S. Wang, K. Murata, T. Hayakawa, S. Hamakawa, K. Suzuki, Appl. Catal. A 196 (2000) 1.
[27] S. Wang, K. Murata, T. Hayakawa, S. Hamakawa, K. Suzuki, Catal. Lett. 63 (1999) 59.
[28] K. Takehira, Y. Ohishi, T. Shishido, T. Kawabata, K. Takaki, Q. Zhang, Y. Wang, J. Catal. 224 (2004) 404.
[29] Y. Ohishi, T. Kawabata, T. Shishido, K. Takaki, Q. Zhang, Y. Wang, K. Takehira, J. Mol. Catal. A 230 (2005) 49.
[30] I. Takahara, W.-C. Chang, N. Mimura, M. Saito, Catal. Today 45 (1998) 55.